bioRχiv

Functional redundancy and formin-independent localization of tropomyosin isoforms in *Saccharomyces cerevisiae*

Anubhav Dhar[a,c], Bagyashree VT[a,c], Sudipta Biswas[b], Jayanti Kumari[a], Amruta Sridhara[a], Jeevan Subodh B[a], Shashank Shekhar[b], Saravanan Palani[a*]
[a]Department of Biochemistry, Indian Institute of Science, Bengaluru, Karnataka 560012, India
[b]Departments of Physics, Cell Biology and Biochemistry, Emory University, Atlanta, GA, 30322, USA
[c]equal contribution
[*]Correspondence: spalani@iisc.ac.in

Abstract

Tropomyosin is an actin binding protein which protects actin filaments from cofilin-mediated disassembly. Distinct tropomyosin isoforms have long been hypothesized to differentially sort to subcellular actin networks and impart distinct functionalities. Nevertheless, a mechanistic understanding of the interplay between Tpm isoforms and their functional contributions to actin dynamics has been lacking. In this study, we present acetylation-mimic engineered mNeonGreen-Tpm fusion proteins that exhibit complete functionality as a sole copy, surpassing limitations of existing probes and enabling real-time dynamic tracking of Tpm-actin filaments *in vivo*. Using these functional Tpm fusion proteins, we find that both Tpm1 and Tpm2 indiscriminately bind to actin filaments nucleated by either formin isoform- Bnr1 and Bni1 *in vivo*, in contrast to the long-held paradigm of Tpm-formin pairing. We also show that Tpm2 can protect and organize functional actin cables in absence of Tpm1. Overall, our work supports a concentration-dependent and formin-independent model of Tpm-actin binding and demonstrates for the first time, the functional redundancy of the paralog Tpm2 in actin cable maintenance in *S. cerevisiae.*

Introduction

Tropomyosins (Tpm) are a major class of actin-binding proteins present in fungi[1] and metazoans[2–4]. Tropomyosins are helical coiled-coil proteins that form head-to-tail dimers and co-polymerize with actin filaments[5,6,6–8]. Tpm was initially discovered as a component of muscle[9] where it regulates actomyosin contraction[10,11]. Later studies revealed that Tpm isoforms are also abundant in non-muscle cells[4,12–14] and even single-celled eukaryotic organisms like fungi[13,15,16]. The canonical role of non-muscle Tpm is to stabilize and protect actin filaments from actin-severing proteins like cofilin[17–19] and thus regulate turnover of actin networks[20]. Tpm display a great diversity of isoforms across species with involvement in various cellular processes such as cell motility[21], cell division[13], organellar movement, secretory vesicle delivery, etc.[2–4,22] Mammals have four tropomyosin genes which produce around 40 isoforms via alternate splicing[35,52]. Various studies have shown that Tpm isoforms sort extensively to distinct actin filament subpopulations and define diverse functionalities for these networks by controlling the interactions between F-actin and other actin-binding proteins such as myosin, cofilin, capping protein, etc[2,4,23–25]. The molecular basis for Tpm isoform sorting remains an unresolved question with various mechanisms such as concentration dependence[26] or a formin-dependent targeting[27,28] having been observed. Structural analysis using cryoEM has now revealed that Tpm isoforms may exert differential functions via different modes of binding and controlling accessibility of ABPs like myosin and cofilin to F-actin[29,30]. How Tpm isoforms have been fine-tuned to perform distinct spatial sorting and functions during evolution remains an active area of research and their crosstalk during recruitment and maturation within the same actin structure is just beginning to be understood[21,31].

The eukaryotic model organism *Saccharomyces cerevisiae* has two tropomyosin isoforms encoded by two different genes- *tpm1* and *tpm2*[1,15,16]. Tpm1 (199 amino acids) is considered a duplicated paralog of Tpm2 (161 amino acids) with a 38 amino acid internal duplication[16]. Tpm1 is considered the major isoform and Δ*tpm1* cells display a near complete loss of actin cables and lethality at higher temperatures[13,28,29]. Δ*tpm2* cells on the other hand show no detectable changes in actin cable organization and cell growth[16,32]. Interestingly, deletion of both *tpm1* and *tpm2* is synthetic lethal[16]. Cells compromised in actin severing factors such as Δ*aip1* or Δ*srv2* mutants show partial restoration of cables in Δ*tpm1* cells which suggests that Tpm1 is majorly involved in protection of the actin filaments from severing proteins of the CCA (Cofilin-Coronin-Aip1) complex *in vivo*[33,34]. The minor isoform Tpm2 is expressed at ~5 fold lower levels and Tpm2 overexpression could not restore normal growth and actin cables in Δ*tpm1* cells in a previous study[16]. The *in vivo* functions of Tpm2 have remained unclear but studies have suggested a role for Tpm2 in negatively controlling retrograde actin cable flow (RACF) possibly via regulating actin filament binding of the type-II myosin Myo1, which is positive regulator of RACF[35,36]. Both

Tpm1 and Tpm2 facilitate processive motion of the type-V myosin Myo2 on coated actin filaments *in vitro*[37], contributing to the anterograde flow of organelles and cargo to the growing bud[22,38,39]. Thus, Tpm1 is believed to play a major role in maintaining the actin cytoskeleton in yeast while the functions of Tpm2 are believed to be majorly distinct from Tpm1[16]. While genetic studies have indicated a possible preference between Tpm isoforms and formin isoforms[32], whether Tpm1 and Tpm2 localize to distinct actin filaments/cables in *S. cerevisiae* has remained unaddressed mainly due to absence of functional Tpm fluorescent fusions and live-cell imaging data for Tpm1 and Tpm2. Recent work from our lab made it possible to visualize the live dynamics of Tpm across species using mNG-Tpm fusion proteins[40] and revealed their localization to actin cables and the actomyosin ring during the cell cycle[40]. However, their combined action and roles in actin cable stability *in vivo* have not been fully explored.

In this study, we assess the functionality of mNeonGreen-Tpm fusion proteins and present acetyl-mimic (-am) engineered mNG-amTpm fusion proteins which restore complete functionality and show mild improvements in signal-to-noise ratio during imaging. Using mNG-amTpm fusion proteins, we find that Tpm1 and Tpm2 indiscriminately associate with actin filaments made by either formin Bnr1 and Bni1, unlike the differential association of acetylated and unacetylated Cdc8 to distinct formin-nucleated filament populations shown in *S. pombe*[27,41]. Lastly, we report a novel function of Tpm2 and show that Tpm2 can compensate for loss of Tpm1 upon increased expression *in vivo*. In contrast to the long-held view, we find that increased Tpm2 expression can restore full length actin cables and actin-cable dependent functions such as vesicle targeting to bud and maintenance of normal mitochondrial morphology suggesting that Tpm2 can independently organize a functional actin cable network in *S. cerevisiae* in the absence of Tpm1. Overall, our findings support a concentration-dependent and formin-independent localization of Tpm isoforms to actin cables and unveil the functional redundancy between Tpm isoforms in *S. cerevisiae*.

Results and Discussion

Acetylation-mimic restores complete functionality to mNG-Tpm fusion proteins

Visualization of tropomyosin in live cells has been a major challenge because fluorescently-tagged tropomyosin fusions are not completely functional and thus, need careful interpretation for accurate insights about Tpm localization and dynamics *in vivo*[42]. We have recently shown that mNeonGreen-Tpm (mNG-Tpm) fusion proteins clearly report localization of Tpm isoforms to actin structures *in vivo* in fungal and mammalian cells[40] **(Fig. S1A, S1B)** but their functionality compared to native Tpm remained a question of interest. To address if mNG-Tpm

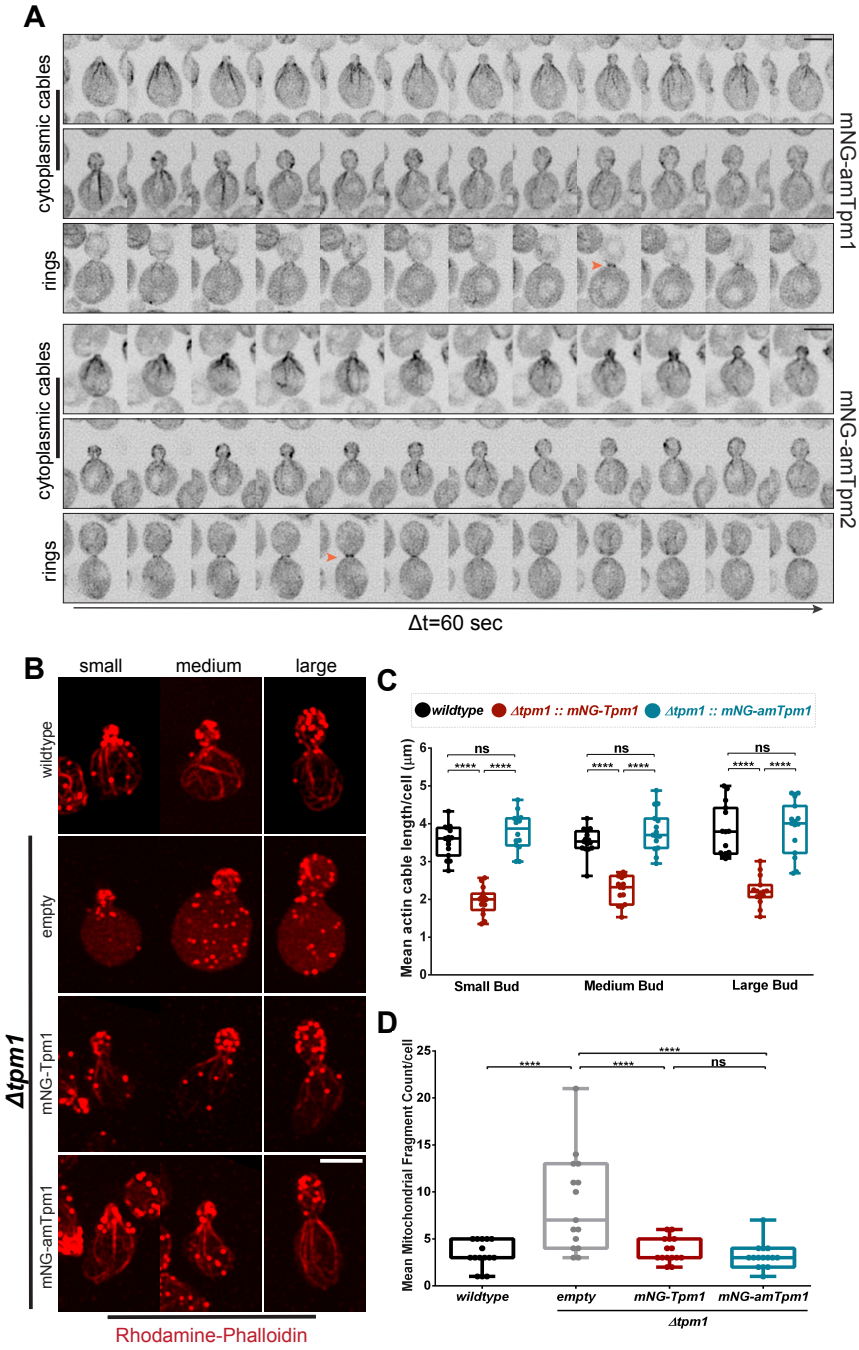

Figure 1: Acetylation-mimic restores complete functionality to mNeonGreen-Tpm fusion proteins. (A) Representative time-lapse montages of wildtype yeast cells expressing mNG-amTpm1 (top) or mNG-amTpm2 (bottom); scale bar - 3µm. **(B)** Representative images of cells of indicated yeast strains stained with Rhodamine-phalloidin; scale bar - 3µm. **(C)** Plot representing mean actin cable length per cell for indicated strains as per experiment shown in (B). **(D)** Plot representing mean mitochondrial fragment count per cell for indicated strains as per experiment shown in S1G.
Box represents 25th and 75th percentile, line represents median, whiskers represent minimum and maximum values

fusion proteins could compensate for loss of native Tpm in cells, we assessed complementation of cellular defects caused by deletion of *tpm1* gene by mNG-Tpm1 expressed under the native *tpm1* promoter. We found that mNG-Tpm1 expression could completely restore normal growth **(Fig. S1C, S1D)** but only partially restore the length of actin cables in Δ*tpm1* cells which exhibit slower growth and absence of actin cables **(Fig. S1E, S1F)**. The presence of shorter actin cables suggests that mNG-Tpm1 fusion is only partially functional as compared to the native Tpm1 protein but can support normal yeast growth probably due to targeting of vesicles to the growing bud cortex. One possible explanation is that lack of N-terminal acetylation of mNG-Tpm by the Nat3-Mdm20 complex which is essential for normal Tpm-actin binding *in vivo*[43–45]. This could result in reduced binding affinities towards F-actin as compared to native Tpm. Thus, we constructed a new mNG-Tpm fusion, mNG-amTpm, wherein we inserted an Ala-Ser dipeptide before the starting methionine of Tpm to mimic the native N-acetylated Tpm[46]. Live-cell imaging of cells expressing mNG-amTpm fusion protein as an integrated single copy showed improved but clear signal enhancement of both mNG-amTpm1 and mNG-amTpm2 on actin cables and the actomyosin ring **(Fig. 1A)**. mNG-amTpm1 expression could completely rescue the growth defects **(Fig. S1C, S1D)** and restore full-length actin cables in Δ*tpm1* cells when expressed at similar levels as mNG-Tpm1 **(Fig. 1B, 1C)**. These results clearly indicate that mNG-amTpm1 is a fully functional tagged tropomyosin with similar activity as native Tpm1. Next, we tested whether actin cables restored by mNG-Tpm1 and mNG-amTpm1 are functional and assessed mitochondrial morphology as a readout of function. We found that mitochondrial fragment number is restored to wildtype levels by expression of both mNG-Tpm1 and mNG-amTpm1 in Δ*tpm1* cells which show hyper-fragmented mitochondria[47,48] **(Fig. 1D, S1G)**.

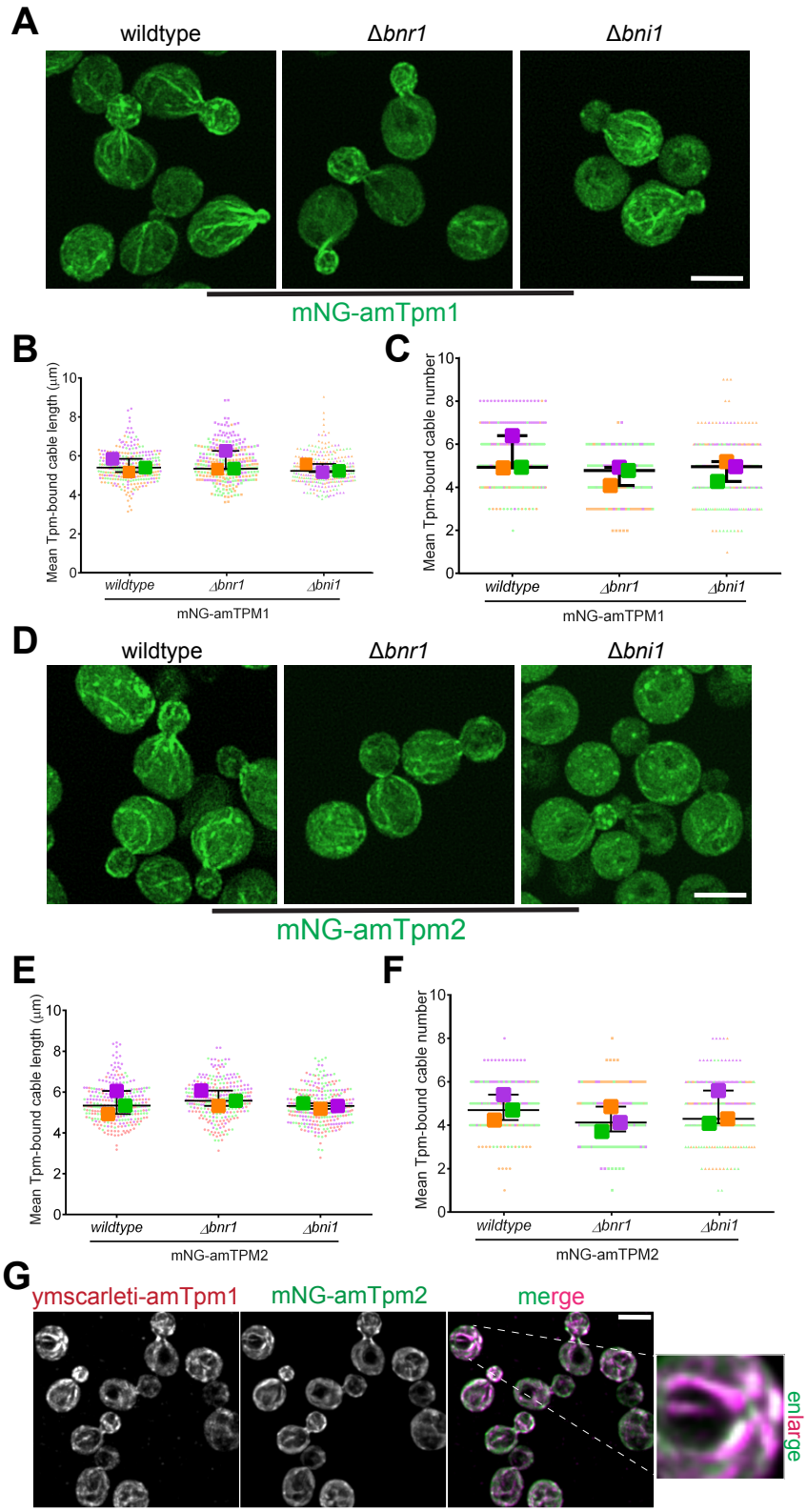

Figure 2: Tpm1 and Tpm2 indiscriminately bind to actin filaments nucleated by formin isoforms, Bnr1 and Bni1. (A) Representative images of cells of wildtype, Δ*bnr1*, and Δ*bni1* cells expressing mNG-amTpm1 fusion protein; scale bar - 3µm. **(B)** Superplot representing mean Tpm-bound cable length per cell in wildtype, Δ*bnr1*, and Δ*bni1* cells expressing mNG-amTpm1; n=100 cells for each strain per replicate, N=3. **(C)** Superplot representing mean Tpm-bound cable number per cell in wildtype, Δ*bnr1*, and Δ*bni1* cells expressing mNG-amTpm1; n=100 cells for each strain per replicate, N=3. **(D)** Representative images of cells of wildtype, Δ*bnr1*, and Δ*bni1* cells expressing mNG-amTpm2 fusion protein; scale bar - 3µm. **(E)** Superplot representing mean Tpm-bound cable length per cell in wildtype, Δ*bnr1*, and Δ*bni1* cells expressing mNG-amTpm2; n=100 cells for each strain per replicate, N=3. **(F)** Superplot representing mean Tpm-bound cable number per cell in wildtype, Δ*bnr1*, and Δ*bni1* cells expressing mNG-amTpm2; n=100 cells for each strain per replicate, N=3. **(G)** Representative images of wildtype yeast cells co-expressing ymScarleti-amTpm1 and mNG-amTpm2; scale bar - 3µm.

Taken together, our results demonstrate that acetylation mimic restores complete functionality of mNG-Tpm proteins and expands their applicability to probe a broad range of questions about Tpm isoform biology.

Tpm1 and Tpm2 indiscriminately bind to actin cables nucleated by both formin isoforms

Tpm isoforms are known to sort to distinct actin filament structures in space and time in various organisms[4,4,23,28,28,29,41,49–53] and the basis of this spatial sorting remains an enigmatic question[26,54]. N-terminal acetylated and unacetylated forms of the fission yeast Tpm, Cdc8, show a formin-dependent spatial sorting to distinct actin cable networks[27,41]. Contrasting results from studies in mammalian cells support both formin-mediated[27,28] or relative concentration-dependent sorting mechanisms[26]. The presence of two Tpm isoforms maintained at distinct expression levels (Tpm1 expressed ~5-6 fold higher than Tpm2)[16,55] and previous observations showing that Δ*tpm1* shows distinct genetic interactions with either formin- Bnr1 and Bni1 indicates a possible crosstalk between Tpm and formin isoforms in *S. cerevisiae*[32]. Tpm1 also increased Bni1-mediated nucleation of actin filaments in an *in vitro* assay without having any effect on Bnr1-mediated nucleation in the same study[32]. However, whether these differences observed *in vitro* translate to measurable effects and possible

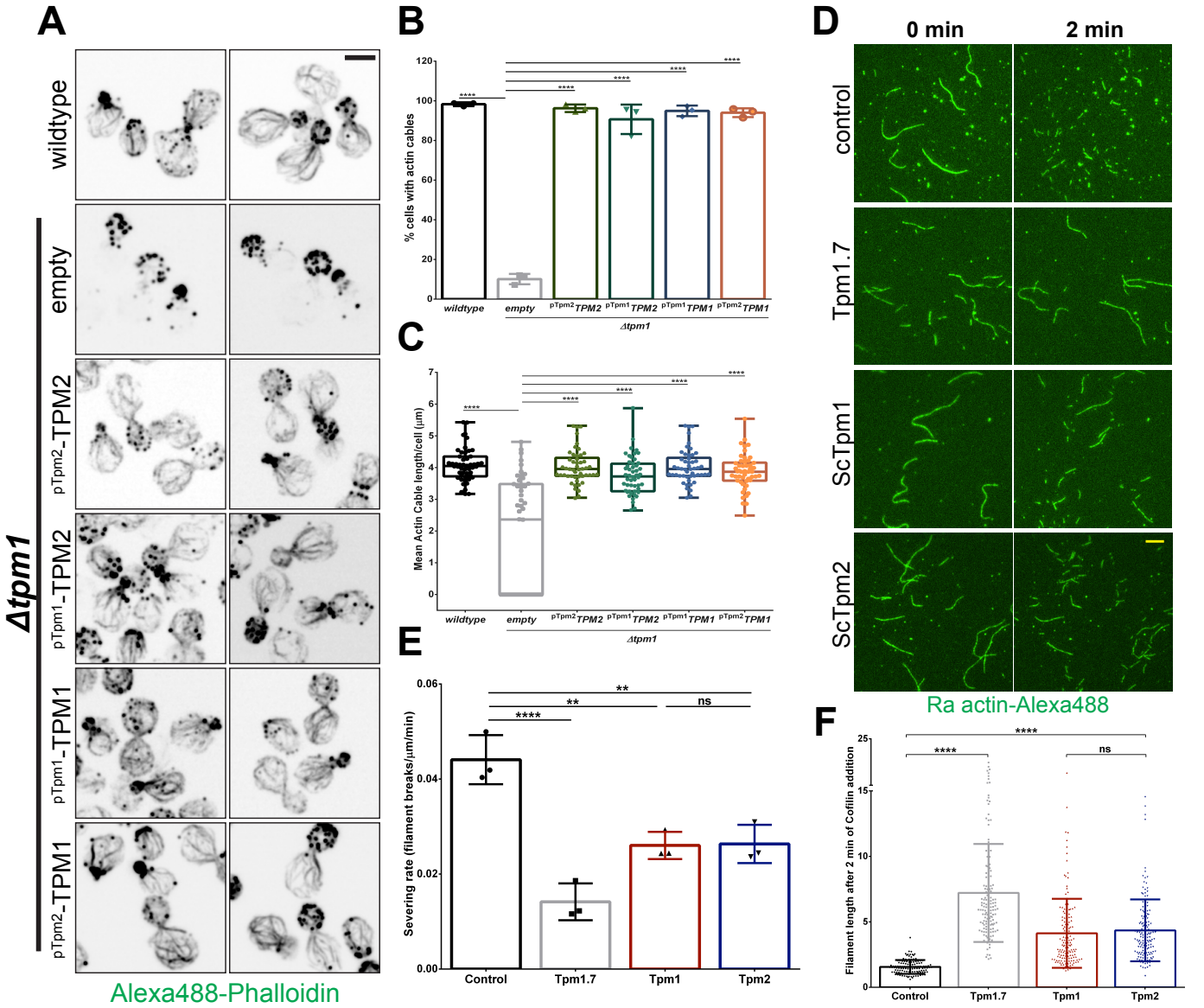

Figure 3: Tpm2 can protect actin filaments from cofilin-mediated severing *in vitro* and *in vivo*. (A) Representative images of indicated yeast strains stained with Alexa488-phalloidin; scale bar – 3µm. **(B)** Plot representing mean percentage of cells with detectable actin cables in indicated yeast strains averaged over 3 biological replicates; n>150 cells for each strain per replicate, N=3. **(C)** Plot representing mean actin cable length per cell in the indicated yeast strains as per experiment in (A); n=50 cells for each strain. **(D)** Representative time-lapse images of the actin filaments before (left) and 2 min after the addition of recombinant ScCofilin (right) in absence or presence of different Tpm isoforms; scale bar - 10µm. **(E)** Plot representing number of severing events per µm of actin filaments per minute. Data shown for independent trials; n≥150 filaments in each condition, N=3. **(F)** Plot representing actin filament lengths after 2 minutes of addition of Cof1 to the samples in absence (control) or presence of specified tropomyosin; n= ~200 filaments, N=3.
*Box represents 25th and 75th percentile, line represents median, whiskers represent minimum and maximum value

formin-based spatial sorting of Tpm1 and Tpm2 *in vivo* remains unclear. To answer these questions, we investigated if Tpm1 and Tpm2 preferred actin cables nucleated by a specific formin isoform - Bnr1 or Bni1. Bnr1 and Bni1 localize to the bud neck and bud cortex respectively from G1 till onset of cytokinesis where they nucleate distinct sets of actin filaments[56–60]. Localization of both Tpm1 and Tpm2 on actin cables could be observed in both Δ*bnr1* and Δ*bni1* **(Fig. 2A, 2D)** cells and also at the fusion focus in mating cells where Bni1 is the sole formin responsible for actin cable nucleation[61,62] **(Fig. S2A, S2B)**. Together, these results qualitatively suggest that both Tpm1 and Tpm2 bind to actin cables nucleated by either formin - Bnr1 and Bni1 indiscriminately.

To assess for any minor biases in preference shown by Tpm1 and Tpm2 for formins Bnr1 and Bni1, we then performed an extensive quantitative analysis of actin cable organization visualized by phalloidin staining **(Fig. S2C, S2F)** and Tpm localization visualized by mNG-amTpm1/2 fusion proteins in wildtype, Δ*bnr1,* and Δ*bni1* cells **(Fig. 2A, 2D)**. However, mNG-amTpm signal drastically weakened after fixation making it difficult to score properly for Tpm localization. Hence, we measured average actin and Tpm-bound actin cable length and number in these strains as a population average instead of simultaneous co-staining in single cells **(Fig. 2A, 2D, S2C, S2F)**. Our analysis revealed that actin cable numbers dropped significantly upon deletion of either formin Bnr1 and Bni1 suggesting a redundant role for both formins in actin cable nucleation, **(Fig. S2E, S2H)** while actin cable lengths were longer in *Δbnr1* as compared to both wildtype and Δ*bni1* cells **(Fig. S2D, S2G)** which could be explained by the elongated cell shape observed in Δ*bnr1* cells **(Fig. S2C, S2F)**. Both Tpm1- and Tpm2-bound cable length did not change significantly between wildtype*,* Δ*bnr1, and* Δ*bni1* cells **(Fig. 2B, 2E)** and number of Tpm1- and Tpm2-bound cables also showed no significant difference between *wildtype,* Δ*bnr1, and* Δ*bni1* cells **(Fig. 2C, 2F)**. Our quantitative analysis suggests that Tpm1 and Tpm2 localization is unaffected by absence of the formin isoforms- Bnr1 and Bni1 and they indiscriminately bind to both Bnr1- and Bni1-nucleated actin cables in *S. cerevisiae.*

Lastly, we assessed if Tpm1 and Tpm2 localize to the same set of actin cables *in vivo* by co-expressing ymScarleti-amTpm1 and mNG-amTpm2 fusion proteins. We observed that both ymScarleti-amTpm1 and mNG-amTpm2 localized to the same set of actin cables **(Fig. 2G)** in cells indicating that they may either co-polymerize on a single actin filament or are bound to different actin filaments bundled together into an actin cable.

Overall, our qualitative and quantitative analysis suggests that Tpm1 and Tpm2 indiscriminately bind to actin filaments nucleated by either formin, Bnr1 and Bni1, and do not exhibit spatial sorting to distinct actin cable networks in *S. cerevisiae*. Since, Tpm1 and Tpm2 are present at different expression levels and cellular concentrations, their relative local concentrations may be the major factor in determining their localization to actin filament networks in *S. cerevisiae* and governing their functions.

Tpm2 overexpression can compensate for loss of Tpm1 function *in vivo*

Tpm1 and Tpm2 isoforms are believed to play both shared and distinct roles in *S. cerevisiae*[16,35]. The major isoform Tpm is expressed 5-6 fold higher than Tpm2 and its absence leads to a near complete loss of actin cables[15,32,63] **(Fig. S3B)**. A previous study reported that overexpression of Tpm2 could not restore actin cables in a Δ*tpm1* strain suggesting that Tpm2 and Tpm1 may have distinct functions[16]. We were intrigued by this observation as Tpm1 and Tpm2 have identical subcellular localization and dynamics as revealed by live-cell imaging of mNG-amTpm fusion proteins **(Fig. 1A, 2G)**. Thus, we decided to revisit Tpm2 functionality and determine its subcellular roles in maintaining the actin cytoskeleton. To assess whether Tpm2 could complement growth defects caused by loss of Tpm1, we overexpressed Tpm2 in a Δ*tpm1* strain using a high-copy number plasmid and surprisingly, found that Tpm2 overexpression could restore growth rates similar to wildtype levels in Δ*tpm1* cells **(Fig. S3A)**. This intriguing finding led us to investigate whether Tpm2 overexpression could also restore actin cables in Δ*tpm1* cells. Interestingly, we observed that Tpm2 overexpression could rescue actin cables similar in length and number to wildtype in ~80% of Δ*tpm1* cells **(Fig. S3B, S3C)**. We confirmed Tpm2 overexpression using RT-qPCR data which revealed a ~19 fold higher Tpm2 mRNA abundance after expression through high-copy number plasmid (pRS425-Tpm2) as compared to Tpm2 mRNA levels in wildtype and Δ*tpm1* cells **(Fig. S3D)**.

This data clearly suggests that in contrary to previous understanding, elevated levels of Tpm2 can organize polarized actin cables in the absence of Tpm1, potentially by protecting actin cables from the severing action of cofilin. This represents a previously unrecognized activity for Tpm2 and raises further interesting questions about the shared and distinct roles of Tpm isoforms in *S. cerevisiae.*

Mild increase in Tpm2 expression can restore actin cable organization in Δ*tpm1* cells

We assessed if increasing Tpm2 protein levels via low-copy plasmid expression under native Tpm1 and Tpm2 promoters (^{ptpm1}Tpm1 and ^{ptpm2}Tpm2) could rescue defects of Δ*tpm1* cells. We assessed their ability to rescue growth of Δ*tpm1* cells and found that both ^{ptpm2}Tpm2 and ^{ptpm1}Tpm2 constructs restored wildtype growth levels in Δ*tpm1* cells **(Fig. S3F)**. Expression of ^{ptpm2}Tpm1 and ^{ptpm1}Tpm1 (positive control) also restored normal growth levels in Δ*tpm1* cells **(Fig. S3F)**. F-actin staining with Alexa488-phalloidin showed rescue of actin cables by all Tpm2 and Tpm1 expression constructs in ~90% Δ*tpm1* cells **(Fig. 3A, 3B)** to similar length as the wildtype **(Fig. 3C)**. To determine the amount of Tpm2 mRNA after expression through low-copy plasmids, we performed RT-qPCR and found that Tpm2 mRNA levels showed ~2 fold average increase when expressed under the *ptpm1* promoter and did not show any detectable change

from wildtype levels when expressed under its native *ptpm2* promoter **(Fig. S3E)**. Wildtype and Δ*tpm1* cells had similar Tpm2 mRNA levels suggesting Tpm2 expression is not sensitive to loss of Tpm1 **(Fig. S3F)**.

To test whether Tpm1 and Tpm2 impart similar protection against cofilin-mediated severing, we performed an in-vitro TIRF imaging[64,65] with purified yeast tropomyosins (Tpm1, Tpm2), human Tpm1.7[66] (positive control) and budding yeast Cofilin (Cof1) **(Fig. 3D)**. We found that Tpm1.7, Tpm1 and Tpm2 coated-actin filaments displayed significantly lower severing events per unit time and length **(Fig. 3E)** and resulted in higher filament lengths after 2 min of cofilin addition as compared to uncoated control filaments **(Fig. 3F)**. These observations suggest that Tpm1 and Tpm2 display similar biochemical activities of actin filament protection from severing action of cofilin and corroborate our *in vivo* observations that Tpm2 can efficiently protect and organize actin filaments as Tpm1.

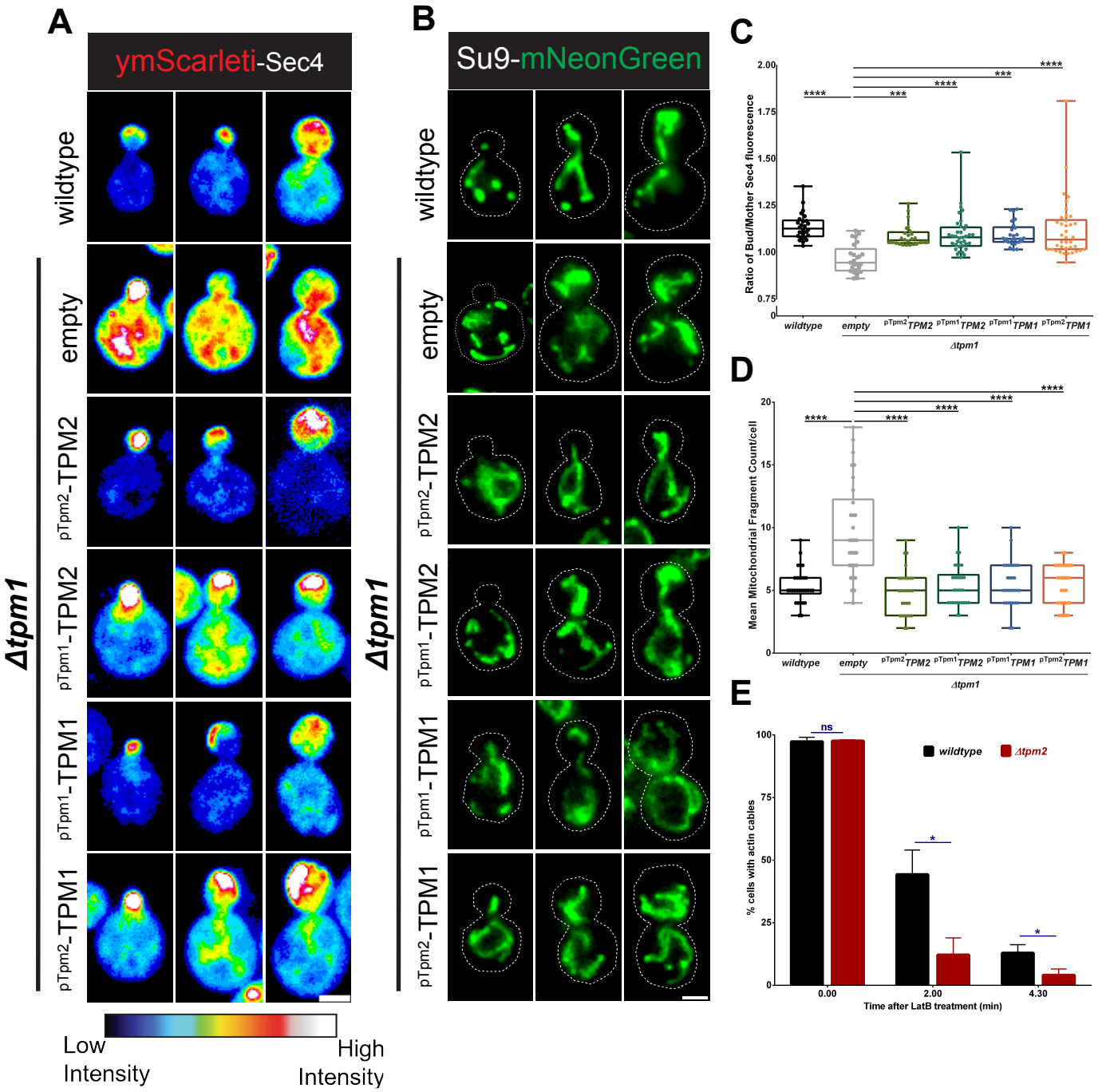

Figure 4: Tpm2 can independently organize a functional actin cytoskeleton in *Δtpm1* cells. (A) Representative images of indicated yeast strains expressing ymScarleti-Sec4; scale bar – 3μm. **(B)** Representative images of indicated yeast strains expressing Su9-mNeonGreen; Scale bar – 3μm. **(C)** Plot representing ratio of bud/mother ymScarleti-Sec4 fluorescence per cell in the indicated yeast strains; n≥25 cells per strain. **(D)** Plot representing mean mitochondrial fragment count per cell in the indicated yeast strains; n≥30 cells per strain. **(E)** Plot representing mean percentage of cells with detectable actin cables in indicated yeast strains averaged over 3 biological replicates; n>125 cells per strain per replicate, N=3.
*Box represents 25th and 75th percentile, line represents median, whiskers represent minimum and maximum value

These results show that even a doubling in Tpm2 expression can restore normal actin cable organization in Δ*tpm1* cells suggesting that Tpm2 protein is present at limiting levels but retains the function of actin cable protection from severing factors like cofilin *in vivo* and *in vitro*. Tpm2 can, therefore, act as a safeguard mechanism for cells to protect against defects in Tpm1 and provides functional redundancy for actin cable maintenance in *S. cerevisiae.*

Tpm2 can solely organize a functional actin cable network in *S. cerevisiae*

Actin cables in *S. cerevisiae* are required for functions such as anterograde transport of vesicles and organelles[22,32,37,56,57,63], maintenance of mitochondrial inheritance and morphology[47,48,67,68], and clearance of protein aggregates from the bud[69,70] while retaining damaged mitochondria in the mother via retrograde actin cable flow (RACF)[36,71]. We asked whether Tpm2 organized actin cables could perform all these functions and if Tpm1-organized and Tpm2- organized actin cable networks had functional differences. We systematically analyzed these functional readouts using fluorescent reporters in wildtype, Δ*tpm1*, and Δ*tpm1* cells expressing Tpm2 in low-copy number and high-copy number plasmids. We used exogenous expressed ymScarleti-Sec4[32] integrated into the *ura3/leu2* locus to assess vesicle targeting to the bud via Myo2-dependent transport on actin cables[22] **(Fig. 4A, S4A)**. The ratio of bud-to-mother Sec4 fluorescence was calculated for all strains and the results showed that vesicle targeting to the bud was restored to levels similar to wildtype cells by expression of both ^{ptpm2}Tpm2 and ^{ptpm1}Tpm2 constructs **(Fig. 4C, S4C)**. Tpm1 expression also rescued vesicle targeting as a positive control under p*tpm1* and p*tpm2* promoters **(Fig. 4A, 4C, S4C)**. These results suggest that both Tpm2 and Tpm1 can individually facilitate normal anterograde flow of cargo and vesicles to the growing bud via facilitation of Myo2 processivity on actin cables, in agreement with previous *in vitro* experiments where both Tpm1 and Tpm2 increased processivity of the type-V myosin, Myo2, on coated actin filaments[37].

Next, we assessed whether the hyper-fragmented mitochondrial morphology, a characteristic of Δ*tpm1* cells[47,48], could be restored by exogenous expression of Tpm2. For visualization of mitochondrial morphology, we used Su9-mNeonGreen[72] (subunit 9 of the F1-F0 ATPase fused to mNeonGreen) construct integrated at the *leu2/ura3* locus and quantified average mitochondrial fragment number per cell **(Fig. 4B, S4B)**. Δ*tpm1* cells showed increased mean mitochondrial fragment number as compared to wildtype while expression of Tpm2 or Tpm1 under native promoters in low copy or high copy plasmids restored the average mitochondrial fragment number to wildtype levels **(Fig. 4D, S4D)**. These results suggest that Tpm2-bound actin cables can interact and crosstalk normally with mitochondria to maintain its normal morphology. The underlying mechanisms of how actin cables control mitochondrial morphology in budding yeast remain largely unknown and future studies are required to understand this enigmatic phenomenon.

Tpm2 has been previously implicated in negative regulation of retrograde actin cable flow (RACF) rates, possibly via its inhibitory effect on binding of the type-II myosin (Myo1) to actin filaments[35,36]. We independently replicated this experiment using Abp140-yeGFP[35,71] as an actin cable marker and corroborated that RACF rates are increased in the absence of Tpm2 and exogenous expression of Tpm2 in Δ*tpm2* cells restores RACF rates to wildtype levels **(Fig. S4E, S4F)**. These observations suggest that Tpm2 has gained distinct regulatory function from Tpm1 in negatively regulating RACF while retaining its actin protective activity.

Next, to test whether actin cable sensitivity is affected in cells lacking Tpm2, we assessed the presence of actin cables after treatment with the actin monomer sequestering drug, Latrunculin B (LatB) **(Fig. S4G)**. We found that Δ*tpm2* cells are significantly more sensitive to the depolymerizing effect of LatB than wildtype cells **(Fig. 4E)**, suggesting that Tpm2 does play previously unrecognized detectable roles in actin cable stability in conditions of stress and contributes to actin cable robustness.

Overall, our results suggest that Tpm2 can independently organize a functional actin cytoskeleton in *S. cerevisiae*. Our work highlights a previously unappreciated function of Tpm2 and demonstrates functional redundancy between Tpm isoforms despite evolutionary divergence and evolution of distinct functions such as RACF regulation. This functional redundancy may benefit cells under stress conditions and contribute to robust cell survival and viability.

In summary, our work presents the first completely functional fluorescently tagged-tropomyosin fusion proteins which have allowed us for the first time to probe tropomyosin isoform localization, functions, and competition with other actin-binding proteins in live cells. We demonstrate their utility by addressing the long-standing question of Tpm isoform sorting in the model *S. cerevisiae* and find a formin-independent mode of binding of Tpm isoforms to actin cables, in contrast to the formin-dependent modes observed in *S. pombe*[27]. Our data suggests distinct evolutionary adaptations and strategies for Tpm isoform sorting across species, contingent on species-specific needs. Our work also addresses the question of functional divergence of Tpm isoforms where we report a previously unknown role of the "minor" isoform Tpm2 in actin cable protection suggesting that Tpm2 has retained its actin protective function despite evolutionary divergence and gain of distinct regulatory activity in controlling retrograde actin cable flow as compared to Tpm1[35]. Our data suggests that such functional redundancy among diverged Tpm isoforms may confer robustness to actin-dependent processes and increase chances of cell survival under certain stressed conditions. In the future, it remains to be understood whether structural differences in F-actin binding modes[30] or other factors such as post-translational modifications[24,44], expression levels and spatio-temporal regulation, etc. contribute to the shared and distinct

roles of closely related Tpm isoforms in *S. cerevisiae* and other eukaryotes.

References

1. Pruyne, D. (2008). Tropomyosin Function in Yeast. In Tropomyosin, P. Gunning, ed. (Springer), pp. 168–186. 10.1007/978-0-387-85766-4_14.
2. Gunning, P., O'Neill, G., and Hardeman, E. (2008). Tropomyosin-based regulation of the actin cytoskeleton in time and space. Physiol Rev *88*, 1–35. 10.1152/physrev.00001.2007.
3. Hitchcock-DeGregori, S.E., and Barua, B. (2017). Tropomyosin Structure, Function, and Interactions: A Dynamic Regulator. Subcell Biochem *82*, 253–284. 10.1007/978-3-319-49674-0_9.
4. Gunning, P.W., Hardeman, E.C., Lappalainen, P., and Mulvihill, D.P. (2015). Tropomyosin - master regulator of actin filament function in the cytoskeleton. J Cell Sci *128*, 2965–2974. 10.1242/jcs.172502.
5. von der Ecken, J., Müller, M., Lehman, W., Manstein, D.J., Penczek, P.A., and Raunser, S. (2015). Structure of the F-actin–tropomyosin complex. Nature *519*, 114–117. 10.1038/nature14033.
6. Obeidy, P., Sobey, T., Nicovich, P.R., Coster, A.C.F., and Pandzic, E. (2021). Tropomyosin isoforms segregate into distinct clusters on single actin filaments (Biophysics) 10.1101/2021.07.23.453476.
7. Bailey, K. (1953). The Structure of Tropomyosin. Proceedings of the Royal Society of London. Series B, Biological Sciences *141*, 45–48.
8. Cohen, C., and Longley, W. (1966). Tropomyosin Paracrystals Formed by Divalent Cations. Science *152*, 794–796. 10.1126/science.152.3723.794.
9. Bailey, K. (1946). Tropomyosin: a New Asymmetric Protein Component of Muscle. Nature *157*, 368–369. 10.1038/157368b0.
10. McKillop, D.F., and Geeves, M.A. (1993). Regulation of the interaction between actin and myosin subfragment 1: evidence for three states of the thin filament. Biophys J *65*, 693–701.
11. Marston, S., and El-Mezgueldi, M. (2008). Role of Tropomyosin in the Regulation of Contraction in Smooth Muscle. In Tropomyosin, P. Gunning, ed. (Springer), pp. 110–123. 10.1007/978-0-387-85766-4_9.
12. Manstein, D.J., Meiring, J.C.M., Hardeman, E.C., and Gunning, P.W. (2020). Actin–tropomyosin distribution in non-muscle cells. J Muscle Res Cell Motil *41*, 11–22. 10.1007/s10974-019-09514-0.
13. Balasubramanian, M.K., Helfman, D.M., and Hemmingsen, S.M. (1992). A new tropomyosin essential for cytokinesis in the fission yeast S. pombe. Nature *360*, 84–87. 10.1038/360084a0.
14. Vrhovski, B., Thézé, N., and Thiébaud, P. (2008). Structure and evolution of tropomyosin genes. Adv Exp Med Biol *644*, 6–26. 10.1007/978-0-387-85766-4_2.
15. Liu, H.P., and Bretscher, A. (1989). Disruption of the single tropomyosin gene in yeast results in the disappearance of actin cables from the cytoskeleton. Cell *57*, 233–242. 10.1016/0092-8674(89)90961-6.
16. Drees, B., Brown, C., Barrell, B.G., and Bretscher, A. (1995). Tropomyosin is essential in yeast, yet the TPM1 and TPM2 products perform distinct functions. J Cell Biol *128*, 383–392. 10.1083/jcb.128.3.383.
17. Bernstein, B.W., and Bamburg, J.R. (1982). Tropomyosin binding to F-actin protects the F-actin from disassembly by brain actin-depolymerizing factor (ADF). Cell Motility *2*, 1–8. 10.1002/cm.970020102.
18. Ono, S., and Ono, K. (2002). Tropomyosin inhibits ADF/cofilin-dependent actin filament dynamics. J Cell Biol *156*, 1065–1076. 10.1083/jcb.200110013.
19. Robaszkiewicz, K., Ostrowska, Z., Marchlewicz, K., and Moraczewska, J. (2016). Tropomyosin isoforms differentially modulate the regulation of actin filament polymerization and depolymerization by cofilins. The FEBS Journal *283*, 723–737. 10.1111/febs.13626.
20. Goode, B.L., Eskin, J., and Shekhar, S. (2023). Mechanisms of actin disassembly and turnover. J Cell Biol *222*, e202309021. 10.1083/jcb.202309021.
21. Brayford, S., Bryce, N.S., Schevzov, G., Haynes, E.M., Bear, J.E., Hardeman, E.C., and Gunning, P.W. (2016). Tropomyosin Promotes Lamellipodial Persistence by Collaborating with Arp2/3 at the Leading Edge. Curr Biol *26*, 1312–1318. 10.1016/j.cub.2016.03.028.
22. Pruyne, D.W., Schott, D.H., and Bretscher, A. (1998). Tropomyosin-containing actin cables direct the Myo2p-dependent polarized delivery of secretory vesicles in budding yeast. J Cell Biol *143*, 1931–1945. 10.1083/jcb.143.7.1931.
23. Reindl, T., Giese, S., Greve, J.N., Reinke, P.Y., Chizhov, I., Latham, S.L., Mulvihill, D.P., Taft, M.H., and Manstein, D.J. (2022). Distinct actin–tropomyosin cofilament populations drive the functional diversification of cytoskeletal myosin motor complexes. iScience *25*, 104484. 10.1016/j.isci.2022.104484.
24. Palani, S., Köster, D.V., Hatano, T., Kamnev, A., Kanamaru, T., Brooker, H.R., Hernandez-Fernaud, J.R., Jones, A.M.E., Millar, J.B.A., Mulvihill, D.P., et al. (2019). Phosphoregulation of tropomyosin is crucial for actin cable turnover and division site placement. J Cell Biol *218*, 3548–3559. 10.1083/jcb.201809089.
25. Boiero Sanders, M., Antkowiak, A., and Michelot, A. (2020). Diversity from similarity: cellular strategies for assigning particular identities to actin filaments and networks. Open Biology *10*, 200157. 10.1098/rsob.200157.
26. Meiring, J.C.M., Bryce, N.S., Niño, J.L.G., Gabriel, A., Tay, S.S., Hardeman, E.C., Biro, M., and Gunning, P.W. (2019). Tropomyosin concentration but not formin nucleators mDia1 and mDia3 determines the level of tropomyosin incorporation into actin filaments. Sci Rep *9*, 6504. 10.1038/s41598-019-42977-2.
27. Johnson, M., East, D.A., and Mulvihill, D.P. (2014). Formins Determine the Functional Properties of Actin Filaments in Yeast. Current Biology *24*, 1525–1530. 10.1016/j.cub.2014.05.034.
28. Zhao, S., Cai, J., Zhang, X., Cui, J., and Jiu, Y. (2020). Different formins restrict localization of distinct tropomyosins on dorsal stress fibers in osteosarcoma cells. Cytoskeleton *77*, 16–24. 10.1002/cm.21588.
29. Gateva, G., Kremneva, E., Reindl, T., Kotila, T., Kogan, K., Gressin, L., Gunning, P.W., Manstein, D.J., Michelot, A., and Lappalainen, P. (2017). Tropomyosin Isoforms Specify Functionally Distinct Actin Filament Populations In Vitro. Current Biology *27*, 705–713. 10.1016/j.cub.2017.01.018.
30. Selvaraj, M., Kokate, S.B., Reggiano, G., Kogan, K., Kotila, T., Kremneva, E., DiMaio, F., Lappalainen, P., and Huiskonen, J.T. (2023). Structural basis underlying specific biochemical activities of non-muscle tropomyosin isoforms. Cell Reports *42*, 111900. 10.1016/j.celrep.2022.111900.
31. Kumari, R., Ven, K., Chastney, M., Peränen, J., Aaron, J., Almeida-Souza, L., Kremneva, E., Poincloux, R., Chew, T.-L., Gunning, P.W., et al. (2023). Specialized actin nanoscale layers control focal adhesion turnover. Preprint at bioRxiv, 10.1101/2023.02.15.528622 10.1101/2023.02.15.528622.
32. Alioto, S.L., Garabedian, M.V., Bellavance, D.R., and Goode, B.L. (2016). Tropomyosin and Profilin Cooperate to Promote Formin-Mediated Actin Nucleation and Drive Yeast Actin Cable Assembly. Curr Biol *26*, 3230–3237. 10.1016/j.cub.2016.09.053.
33. Okada, K., Ravi, H., Smith, E.M., and Goode, B.L. (2006). Aip1 and Cofilin Promote Rapid Turnover of Yeast Actin Patches and Cables: A Coordinated Mechanism for Severing and Capping Filaments. Mol Biol Cell *17*, 2855–2868. 10.1091/mbc.E06-02-0135.
34. Chaudhry, F., Breitsprecher, D., Little, K., Sharov, G., Sokolova, O., and Goode, B.L. (2013). Srv2/cyclase-associated protein forms hexameric shurikens that directly catalyze actin filament severing by cofilin. Mol Biol Cell *24*, 31–41. 10.1091/mbc.E12-08-0589.
35. Huckaba, T.M., Lipkin, T., and Pon, L.A. (2006). Roles of type II myosin and a tropomyosin isoform in retrograde actin flow in budding yeast. J Cell Biol *175*, 957–969. 10.1083/jcb.200609155.
36. Higuchi, R., Vevea, J.D., Swayne, T.C., Chojnowski, R., Hill, V., Boldogh, I.R., and Pon, L.A. (2013). Actin Dynamics Affect Mitochondrial Quality Control and Aging in Budding Yeast. Current Biology *23*, 2417–2422. 10.1016/j.cub.2013.10.022.
37. Hodges, A.R., Krementsova, E.B., Bookwalter, C.S., Fagnant, P.M., Sladewski, T.E., and Trybus, K.M. (2012). Tropomyosin is essential for processive movement of a class V myosin from budding yeast. Curr Biol *22*, 1410–1416. 10.1016/j.cub.2012.05.035.
38. Altmann, K., Frank, M., Neumann, D., Jakobs, S., and Westermann, B. (2008). The class V myosin motor protein, Myo2, plays a major role in mitochondrial motility in Saccharomyces cerevisiae. The Journal of Cell Biology *181*, 119. 10.1083/jcb.200709099.
39. Johnston, G.C., Prendergast, J.A., and Singer, R.A. (1991). The Saccharomyces cerevisiae MYO2 gene encodes an essential myosin for vectorial transport of vesicles. J Cell Biol *113*, 539–551. 10.1083/jcb.113.3.539.

40. Hatano, T., Lim, T.C., Billault-Chaumartin, I., Dhar, A., Gu, Y., Massam-Wu, T., Scott, W., Adishesha, S., Chapa-y-Lazo, B., Springall, L., et al. (2022). mNG-tagged fusion proteins and nanobodies to visualize tropomyosins in yeast and mammalian cells. Journal of Cell Science *135*, jcs260288. 10.1242/jcs.260288.
41. Coulton, A.T., East, D.A., Galinska-Rakoczy, A., Lehman, W., and Mulvihill, D.P. (2010). The recruitment of acetylated and unacetylated tropomyosin to distinct actin polymers permits the discrete regulation of specific myosins in fission yeast. J Cell Sci *123*, 3235–3243. 10.1242/jcs.069971.
42. Brooker, H.R., Geeves, M.A., and Mulvihill, D.P. (2016). Analysis of biophysical and functional consequences of tropomyosin–fluorescent protein fusions. FEBS Letters *590*, 3111–3121. 10.1002/1873-3468.12346.
43. Polevoda, B., Cardillo, T.S., Doyle, T.C., Bedi, G.S., and Sherman, F. (2003). Nat3p and Mdm20p Are Required for Function of Yeast NatB Nα-terminal Acetyltransferase and of Actin and Tropomyosin*. Journal of Biological Chemistry *278*, 30686–30697. 10.1074/jbc.M304690200.
44. Singer, J.M., and Shaw, J.M. (2003). Mdm20 protein functions with Nat3 protein to acetylate Tpm1 protein and regulate tropomyosin–actin interactions in budding yeast. Proceedings of the National Academy of Sciences *100*, 7644–7649. 10.1073/pnas.1232343100.
45. Maytum, R., Geeves, M.A., and Konrad, M. (2000). Actomyosin regulatory properties of yeast tropomyosin are dependent upon N-terminal modification. Biochemistry *39*, 11913–11920. 10.1021/bi000977g.
46. Monteiro, P.B., Lataro, R.C., Ferro, J.A., and Reinach, F. de C. (1994). Functional alpha-tropomyosin produced in Escherichia coli. A dipeptide extension can substitute the amino-terminal acetyl group. J Biol Chem *269*, 10461–10466.
47. Simon, V. r., Karmon, S. l., and Pon, L. a. (1997). Mitochondrial inheritance: Cell cycle and actin cable dependence of polarized mitochondrial movements in Saccharomyces cerevisiae. Cell Motility *37*, 199–210. 10.1002/(SICI)1097-0169(1997)37:3<199::AID-CM2>3.0.CO;2-2.
48. Drubin, D.G., Jones, H.D., and Wertman, K.F. (1993). Actin structure and function: roles in mitochondrial organization and morphogenesis in budding yeast and identification of the phalloidin-binding site. Mol Biol Cell *4*, 1277–1294. 10.1091/mbc.4.12.1277.
49. Janco, M., Bonello, T.T., Byun, A., Coster, A.C.F., Lebhar, H., Dedova, I., Gunning, P.W., and Böcking, T. (2016). The impact of tropomyosins on actin filament assembly is isoform specific. Bioarchitecture *6*, 61–75. 10.1080/19490992.2016.1201619.
50. Bryce, N.S., Schevzov, G., Ferguson, V., Percival, J.M., Lin, J.J.-C., Matsumura, F., Bamburg, J.R., Jeffrey, P.L., Hardeman, E.C., Gunning, P., et al. (2003). Specification of actin filament function and molecular composition by tropomyosin isoforms. Mol Biol Cell *14*, 1002–1016. 10.1091/mbc.e02-04-0244.
51. Percival, J.M., Hughes, J.A.I., Brown, D.L., Schevzov, G., Heimann, K., Vrhovski, B., Bryce, N., Stow, J.L., and Gunning, P.W. (2004). Targeting of a Tropomyosin Isoform to Short Microfilaments Associated with the Golgi Complex. MBoC *15*, 268–280. 10.1091/mbc.e03-03-0176.
52. Goins, L.M., and Mullins, R.D. (2015). A novel tropomyosin isoform functions at the mitotic spindle and Golgi in Drosophila. Mol Biol Cell *26*, 2491–2504. 10.1091/mbc.E14-12-1619.
53. Veeranan-Karmegam, R., Boggupalli, D.P., Liu, G., and Gonsalvez, G.B. (2016). A new isoform of Drosophila non-muscle Tropomyosin 1 interacts with Kinesin-1 and functions in oskar mRNA localization. J Cell Sci *129*, 4252–4264. 10.1242/jcs.194332.
54. Martin, C., Schevzov, G., and Gunning, P. (2010). Alternatively spliced N-terminal exons in tropomyosin isoforms do not act as autonomous targeting signals. J Struct Biol *170*, 286–293. 10.1016/j.jsb.2009.12.016.
55. Gonzalez Rodriguez, S., Wirshing, A.C.E., Goodman, A.L., and Goode, B.L. (2023). Cytosolic concentrations of actin binding proteins and the implications for in vivo F-actin turnover. J Cell Biol *222*, e202306036. 10.1083/jcb.202306036.
56. Sagot, I., Klee, S.K., and Pellman, D. (2002). Yeast formins regulate cell polarity by controlling the assembly of actin cables. Nat Cell Biol *4*, 42–50. 10.1038/ncb719.
57. Evangelista, M., Pruyne, D., Amberg, D.C., Boone, C., and Bretscher, A. (2002). Formins direct Arp2/3-independent actin filament assembly to polarize cell growth in yeast. Nat Cell Biol *4*, 32–41. 10.1038/ncb718.
58. Pruyne, D., Gao, L., Bi, E., and Bretscher, A. (2004). Stable and Dynamic Axes of Polarity Use Distinct Formin Isoforms in Budding Yeast. MBoC *15*, 4971–4989. 10.1091/mbc.e04-04-0296.
59. Buttery, S.M., Yoshida, S., and Pellman, D. (2007). Yeast Formins Bni1 and Bnr1 Utilize Different Modes of Cortical Interaction during the Assembly of Actin Cables. Mol Biol Cell *18*, 1826–1838. 10.1091/mbc.E06-09-0820.
60. Bretscher, A. (2013). Deconstructing formin-dependent actin cable assembly. Proceedings of the National Academy of Sciences *110*, 18744–18745. 10.1073/pnas.1318683110.
61. Evangelista, M., Blundell, K., Longtine, M.S., Chow, C.J., Adames, N., Pringle, J.R., Peter, M., and Boone, C. (1997). Bni1p, a Yeast Formin Linking Cdc42p and the Actin Cytoskeleton During Polarized Morphogenesis. Science *276*, 118–122. 10.1126/science.276.5309.118.
62. Matheos, D., Metodiev, M., Muller, E., Stone, D., and Rose, M.D. (2004). Pheromone-induced polarization is dependent on the Fus3p MAPK acting through the formin Bni1p. J Cell Biol *165*, 99–109. 10.1083/jcb.200309089.
63. Liu, H., and Bretscher, A. (1992). Characterization of TPM1 disrupted yeast cells indicates an involvement of tropomyosin in directed vesicular transport. J Cell Biol *118*, 285–299. 10.1083/jcb.118.2.285.
64. Smith, B.A., Gelles, J., and Goode, B.L. (2014). Single-Molecule Studies of Actin Assembly and Disassembly Factors. Methods Enzymol *540*, 95–117. 10.1016/B978-0-12-397924-7.00006-6.
65. Shekhar, S., and Carlier, M.-F. (2016). Single-filament kinetic studies provide novel insights into regulation of actin-based motility. MBoC *27*, 1–6. 10.1091/mbc.E15-06-0352.
66. Jansen, S., and Goode, B.L. (2019). Tropomyosin isoforms differentially tune actin filament length and disassembly. MBoC *30*, 671–679. 10.1091/mbc.E18-12-0815.
67. Lazzarino, D.A., Boldogh, I., Smith, M.G., Rosand, J., and Pon, L.A. (1994). Yeast mitochondria contain ATP-sensitive, reversible actin-binding activity. Mol Biol Cell *5*, 807–818. 10.1091/mbc.5.7.807.
68. Boldogh, I.R., and Pon, L.A. (2006). Interactions of mitochondria with the actin cytoskeleton. Biochim Biophys Acta *1763*, 450–462. 10.1016/j.bbamcr.2006.02.014.
69. Liu, B., Larsson, L., Caballero, A., Hao, X., Öling, D., Grantham, J., and Nyström, T. (2010). The Polarisome Is Required for Segregation and Retrograde Transport of Protein Aggregates. Cell *140*, 257–267. 10.1016/j.cell.2009.12.031.
70. Liu, B., Larsson, L., Franssens, V., Hao, X., Hill, S.M., Andersson, V., Höglund, D., Song, J., Yang, X., Öling, D., et al. (2011). Segregation of protein aggregates involves actin and the polarity machinery. Cell *147*, 959–961. 10.1016/j.cell.2011.11.018.
71. Yang, H.-C., and Pon, L.A. (2002). Actin cable dynamics in budding yeast. Proceedings of the National Academy of Sciences *99*, 751–756. 10.1073/pnas.022462899.
72. Dua, N., Seshadri, A., and Badrinarayanan, A. (2022). DarT-mediated mtDNA damage induces dynamic reorganization and selective segregation of mitochondria. J Cell Biol *221*, e202205104. 10.1083/jcb.202205104.
73. Sikorski, R.S., and Hieter, P. (1989). A system of shuttle vectors and yeast host strains designed for efficient manipulation of DNA in Saccharomyces cerevisiae. Genetics *122*, 19–27. 10.1093/genetics/122.1.19.
74. Janke, C., Magiera, M.M., Rathfelder, N., Taxis, C., Reber, S., Maekawa, H., Moreno-Borchart, A., Doenges, G., Schwob, E., Schiebel, E., et al. (2004). A versatile toolbox for PCR-based tagging of yeast genes: new fluorescent proteins, more markers and promoter substitution cassettes. Yeast *21*, 947–962. 10.1002/yea.1142.
75. McInally, S.G., Kondev, J., and Goode, B.L. (2022). Quantitative Analysis of Actin Cable Length in Yeast. Bio Protoc *12*, e4402. 10.21769/BioProtoc.4402.
76. McInally, S.G., Kondev, J., and Goode, B.L. (2021). Scaling of subcellular actin structures with cell length through decelerated growth. Elife *10*, e68424. 10.7554/eLife.68424.
77. Collart, M.A., and Oliviero, S. (1993). Preparation of Yeast RNA. Current Protocols in Molecular Biology *23*, 13.12.1-13.12.5. 10.1002/0471142727.mb1312s23.
78. Schindelin, J., Arganda-Carreras, I., Frise, E., Kaynig, V., Longair, M., Pietzsch, T., Preibisch, S., Rueden, C., Saalfeld, S., Schmid, B., et al.

(2012). Fiji: an open-source platform for biological-image analysis. Nat Methods 9, 676–682. 10.1038/nmeth.2019.

Acknowledgements

We thank the Department of Biochemistry, Indian Institute of Science for access to DST-FIST imaging and other central facilities. We also thank the Divisional Bioimaging Facility. We are grateful to Mr. Pabitra Sharma for help with image analysis. We thank Prof. PN Rangarajan, Prof. Ramanujam Srinivasan, Prof. Sunil Laxman, Prof. Sachin Kotak, and Prof. Sunish Radhakrishnan for their feedback. AD and JK acknowledge GATE fellowship from IISc. JSB acknowledges KVPY fellowship from IISc. We thank Silvia Jansen for advice on quantification of TIRF microscopy experiments and Blake Miller for help with protein purification. This paper was typeset with the bioRxiv word template by @Chrelli: www.github.com/chrelli/bioRxiv-word-template

Funding

This work was financially supported by a Department of Biotechnology-Wellcome Trust India Alliance intermediate fellowship (IA/I/21/1/505633), SERB SRG grant (SRG/2021/001600) and an Indian Institute of Science (IISc) start-up grant awarded to S.P. S.S. is supported by NIH NIGMS grant R35GM143050.

Competing interest statement

The authors declare no conflict of interest.

Materials and Methods

Plasmid construction

All plasmids used in this study are listed in Supplementary Table 1. Plasmids were constructed by assembling DNA fragments amplified by PCR into restriction endonuclease-digested vectors using NEB Hifi Builder (NewEngland BioLabs; cat.no: E2621L). The plasmids were confirmed with restriction digestion and sequencing.

Yeast Strains construction

All yeast strains used in this study are listed in Supplementary Table 2. S288c genetic background was used for all modifications. Yeast transformation was done using the Lithium Acetate based method as previously described[73]. Deletion and tagging of genes was done using the homologous recombination of PCR cassettes as described previously[74]. The strains were confirmed using colony PCR and fluorescence microscopy.

Live-cell Imaging of tropomyosin isoforms

Yeast strains were grown overnight in Synthetic Complete (SC) Media at 25°C. The overnight culture was used to inoculate a secondary culture which was allowed to grow till mid-log phase. The cells were then adhered on a Concanavalin A-coated glass-bottom dish (Cellvis cat: no: D35C4-20-1.5-N) containing SC media. Images were acquired using the Andor Dragonfly 502 spinning disk confocal system (Oxford Instruments) equipped with a fully-motorized Leica Dmi8 inverted microscope setup. Z-stacks were acquired using a 100x oil objective, captured with the Andor Sona scMOS camera and deconvolved using Andor Fusion software.

Actin cable staining with phalloidin

In order to visualize the actin cables, cells were stained with Alexa488/Rhodamine Phalloidin and imaged using a previously described protocol[75,76]. Briefly, cells were grown at 23ºC until early-mid log phase in Yeast extract/Peptone/2%Glucose (YPD) media. The cells were then fixed twice with 4% paraformaldehyde in YPD and 4% paraformaldehyde in 1x PBS for 45 minutes each and washed thrice with 1x PBS. Rhodamine/Alexa488 phalloidin (Invitrogen cat: no: R415 and cat: no: A12379 respectively) was added to a final concentration of 0.4μM and incubated overnight with rotation at 4ºC. Next day, the cells were washed thrice with 1X PBS. The cells were adhered on 6% Concanavalin A (Sigma cat: no: C2010) coated glass bottom dishes and z-stacks (step size = o.2μm, 31 slices) were acquired using Andor Dragonfly 502 Spinning Disk system and deconvolved using Andor Fusion Software.

Purification and labeling of actin

Rabbit skeletal muscle actin was purified from acetone powder generated from frozen ground hind leg muscle tissue of young rabbits (PelFreez, USA). Lyophilized acetone powder stored at −80 °C was mechanically sheared in a coffee grinder, resuspended in G-buffer (5 mM Tris-HCl pH 7.5, 0.5 mM Dithiothreitol (DTT), 0.2 mM ATP, and 0.1 mM $CaCl_2$), and cleared by centrifugation for 20 min at 50,000 × g. The supernatant was collected and further filtered with the Whatman paper. Actin was then polymerized overnight at 4 °C, slowly stirring, by the addition of 2 mM $MgCl_2$ and 50 mM NaCl to the filtrate. Next morning, NaCl powder was added to a final concentration of 0.6 M, and stirring was continued for another 30 min at 4 °C. F-actin was pelleted by centrifugation for 2.5 hrs at 280,000 × g. The pellet was solubilized by dounce homogenization and dialyzed against G-buffer for 48 h at 4 °C. Monomeric actin was precleared at 435,000 × g and loaded onto a Sephacryl S-200 16/60 gel-filtration column (Cytiva, USA) equilibrated in G-Buffer. Fractions containing actin were stored at 4 °C.

To biotinylate actin, purified G-actin was first dialyzed overnight at 4 °C against G-buffer lacking DTT. The monomeric actin was then polymerized by the addition of an equal volume of 2X labeling buffer (50 mM imidazole pH 7.5, 200 mM KCl, 0.3 mM ATP, 4 mM $MgCl_2$). F-actin was then mixed with a fivefold molar excess of NHS-XX-Biotin (Merck KGaA, Germany) and incubated in the dark for 15 h at 4 °C. F-actin was pelleted by centrifugation at 450,000 × g for 40 min at room temperature, The pellet was rinsed with G-buffer, homogenized with a dounce and dialyzed against G-buffer for 48 h at 4 °C. Biotinylated monomeric actin was purified further on a Sephacryl S-200 16/60 gel-filtration column as above. Aliquots of biotin-actin were snap-frozen in liquid N_2 and stored at −80 °C.

To fluorescently label actin, G-actin was polymerized by dialyzing overnight against modified F-buffer (20 mM PIPES pH 6.9, 0.2 mM $CaCl_2$, 0.2 mM ATP, and 100 mM KCl). F-actin was incubated for 2 h at room temperature with a fivefold molar excess of Alexa-488 NHS ester dye (Thermo Fisher Scientific, USA, cat: no: A20100). F-actin was pelleted by centrifugation at 450,000 × g for 40 min at room temperature, and the pellet was resuspended in G-buffer, homogenized with a dounce and further incubated on ice for 2 h to depolymerize the filaments. The monomeric actin was then re-polymerized on ice for 1 h by the addition of 100 mM KCl and 1 mM $MgCl_2$. F-actin was once again pelleted by centrifugation for 40 min at 450,000 × g at 4 °C. The pellet was homogenized with a dounce and dialyzed overnight at 4 °C against 1 L of G-buffer. Next morning, the solution was precleared by centrifugation at 450,000 × g for 40 min at 4 °C. The supernatant was collected, and concentration and labeling efficiency of actin were determined. Labelled actin was stored at 4 °C.

Purification of profilin

Human profilin-1 was expressed in *E. coli* strain BL21 (pRare) to log phase in LB broth at 37 °C and induced with 1 mM IPTG for 3 h at 37 °C. Cells were then harvested by centrifugation at 15,000 × g at 4 °C and stored at −80 °C. For purification, pellets were thawed and resuspended in 30 mL lysis buffer (50 mM Tris-HCl pH 8, 1 mM DTT, 1 mM PMSF protease inhibitors (0.5 μM each of pepstatin A, antipain, leupeptin, aprotinin, and chymostatin) was added, and the solution was sonicated on ice by a tip sonicator. The lysate was centrifuged for 45 min at 120,000 × g at 4 °C. The supernatant was then passed over 20 ml of Poly-L-proline conjugated beads in a disposable column (Bio-Rad, USA). The beads were first washed at room temperature in wash buffer (10 mM Tris pH 8, 150 mM NaCl, 1 mM EDTA, and 1 mM DTT) and then washed again with two column volumes of 10 mM Tris pH 8, 150 mM NaCl, 1 mM EDTA, 1 mM DTT, and 3 M urea. Protein was then eluted with five column volumes of 10 mM Tris pH 8, 150 mM NaCl, 1 mM EDTA, 1 mM DTT, and 8 M urea. Pooled and concentrated fractions were then dialyzed in 4 L of 2 mM Tris pH 8, 0.2 mM EGTA, 1 mM DTT, and 0.01% NaN3 for 4 h at 4 °C. The dialysis buffer was replaced with fresh 4 L buffer, and the dialysis was continued overnight at 4 °C. The protein was centrifuged for 45 min at 450,000 × g at 4 °C, concentrated, aliquoted, flash-frozen in liquid N2, and stored at −80 °C.

Purification of yeast and human Tpm isoforms

All budding yeast and human tropomyosins were expressed in *E. coli* strain BL21 to log phase in LB broth at 37 °C and induced with 1 mM IPTG for 3 h at 37 °C. Cells were then harvested by centrifugation at 15,000 × g at 4 °C and stored at −80 °C. For purification, pellets were thawed and resuspended in 30 mL lysis buffer (20 mM Tris-HCl pH 7.5, 0.5 M NaCl, 5 mM $MgCl_2$,

1 mM PMSF, protease inhibitors (0.5 μM each of pepstatin A, antipain, leupeptin, aprotinin, and chymostatin)) was added, and the solution was sonicated on ice by a tip sonicator. The lysate was incubated at 80°C for 10 min in a water bath and at room temperature for another 10 min. The lysate was centrifuged for 30 min at 30,000 x g at 4 °C, and the pellet was discarded. The protein was precipitated by adding 0.3M HCl to the supernatant till the pH reached 4.7. The solution was centrifuged for 30 min at 30,000 x g at 4°C. The pellet was resuspended in 25 mL of wash buffer (100 mM Tris-HCl pH 7.5, 0.5 M NaCl, 5 mM $MgCl_2$, 1 mM DTT). The acid precipitation and accompanying centrifugation step were repeated again. The pellet was then resuspended in 25 mL of wash buffer and dialyzed in 2 L of dialysis buffer (20 mM HEPES pH 6.8, 50 mM NaCl, 0.5 mM DTT) overnight at 4 °C. The dialyzed solution was loaded to a 5 ml HiTrap Q HP column (Cytiva). The protein fractions were eluted with a linear gradient of NaCl (50–600 mM). The fractions were analyzed by SDS-PAGE to determine the ones containing Tpm. They were concentrated and further loaded on a Superose 6 gel-filtration column (Cytiva) pre-equilibrated with 20 mM Tris (pH 7.5), 50 mM KCl, 2 mM MgCl2, 1 mM DTT. Peak fractions were collected, concentrated, aliquoted, and flash-frozen in liquid N2 and stored at −80 °C.

Purification of yeast cofilin

His-tagged yeast Cof1 was expressed in *E. coli* strain BL21 to log phase in LB broth at 37 °C and induced with 1 mM IPTG for 3 h at 37 °C. Cells were then harvested by centrifugation at 15,000 × g at 4 °C and stored at −80 °C. For purification, pellets were thawed and resuspended in 30 mL lysis buffer (50 mM phosphate buffer pH 8, 20 mM Imidazole, 0.3 M NaCl, 1 mM PMSF, protease inhibitors) was added, and the solution was sonicated on ice by a tip sonicator. The lysate was centrifuged for 45 min at 120,000 × g at 4 °C. The supernatant was incubated with 2 mL of washed Ni-NTA beads for 2 hrs at 4 °C. The solution was centrifuged at 1000 xg for 5 minutes. The supernatant was removed. The beads were washed 3 times with 10 mL of wash buffer (50 mM Phosphate buffer pH 8, 20 mM Imidazole, 0.3 M NaCl, 1 mM DTT) and subsequently centrifuged at 1000 xg for 2 min each time to remove the supernatant. Protein was then eluted with 1 mL of elution buffer (50 mM phosphate buffer pH 8, 250 mM Imidazole, 0.3 M NaCl, 1 mM DTT). Pooled and concentrated fractions were then loaded on a Superose 6 gel-filtration column (Cytiva) pre-equilibrated with 20 mM HEPES pH 7.5, 50 mM KCl, 0.5 mM DTT. Peak fractions were collected, concentrated, aliquoted, and flash-frozen in liquid N2 and stored at −80 °C.

TIRF microscopy

Glass coverslips (60 × 24 mm; Thermo Fisher Scientific, USA) were first cleaned by sonication in detergent for 20 min, followed by successive sonications in 1 M KOH, 1 M HCl, and ethanol for 20 min each. Coverslips were then washed extensively with H_2O and dried in an N_2 stream. The cleaned coverslips were coated with 2 mg/mL methoxy-polyethylene glycol (mPEG)-silane MW 2000 and 2 μg/mL biotin-PEG-silane MW 3400 (Laysan Bio, USA) in 80% ethanol (pH 2.0) and incubated overnight at 70 °C. Flow cells were assembled by rinsing PEG-coated coverslips with water, drying with N_2, and adhering to μ-Slide VI0.1 (0.1 mm × 17 mm × 1 mm) flow chambers (Ibidi, Germany) with double-sided tape (2.5 cm × 2 mm × 120 μm) and epoxy resin for 5 min (Devcon, USA). Before each reaction, the flow cell was sequentially incubated for 1 min each with 4 μg/ml streptavidin and 1% BSA in 20 mM HEPES pH 7.5 and 50 mM KCl. The flow cell was then equilibrated with TIRF buffer (10 mM imidazole, pH 7.4, 50 mM KCl, 1 mM $MgCl_2$, 1 mM EGTA, 0.2 mM ATP, 10 mM DTT, 2 mM DABCO, and 0.5% methylcellulose [4000 cP]).

Actin filaments were assembled by introducing 1 μM 15% Alexa 488 labelled 0.1% biotinylated actin and 2 μM profilin in the flow cell, with or without 10 μM Tpm. Filaments were allowed to grow for 2 to 3 min. For experiments containing Tpm, the flow cell was then rinsed with TIRF buffer supplemented with 10 μM Tpm to remove free actin. The solution was then replaced with 10 μM Tpm and 150 nM Cof1. For control experiments containing no Tpm, both washing and cofilin addition step had no Tpm in the solution.

Image acquisition and analysis

Single-wavelength time-lapse TIRF imaging was performed on a Nikon-Ti2000 inverted microscope equipped with a 40 mW Argon laser, a 60X TIRF-objective with a numerical aperture of 1.49 (Nikon Instruments Inc., USA), and an IXON LIFE 888 EMCCD camera (Andor Ixon, UK). One pixel was equivalent to 144 × 144 nm. Focus was maintained by the Perfect Focus system (Nikon Instruments Inc., Japan). Time-lapse images were acquired every 2 s using Nikon Elements imaging software (Nikon Instruments Inc., Japan). The sample was excited by a 488 nm laser for imaging.

Images were analyzed in Fiji. The actin severing rates by cofilin in the presence nts as a function of time on filaments in the field of view and divided by the total length of all the filaments to get the normalized severing rates. The average leor absence of different Tpm isoforms were calculated by counting severing evength of the filaments after severing was measured about 2 min after the cofilin flow-in. Data analysis and curve fitting were carried out in Microcal Origin.

RNA extraction and RT-qPCR

Hot phenol method was used to extract RNA from yeast cells[77]. Overnight grown yeast cells were diluted and allowed to grow until OD at 600nm reached 1. Cells were treated with equal volumes of TES and water saturated acidic phenol and precipitated at -80°C to extract RNA. The extracted RNA was then treated with DNAse A and this was used as a template for first strand cDNA synthesis. Following this, qRT-PCR was set up using the cDNA to check the expression levels. Gene specific primers were used to assess the Tpm1 and Tpm2 levels in wild type and different mutant background. TDH1 and PGK1 housekeeping genes were used as controls for all qRT-PCR experiments.

Vesicle delivery to bud

Vesicle delivery was visualized using an N-terminal tagged ymScarleti-Sec4 construct expressed under ADH promoter as an additional copy integrated into the *ura3* locus. Overnight grown yeast cells were diluted and allowed to grow until mid-log phase. Cells were adhered on a Concanavalin A-coated glass bottom dish and z-stacks were acquired with a step size of 0.5μm to cover a range of 6μm. The ratio of ymScarleti-Sec4 intensity in the bud and mother were taken and plotted to assess targeting of vesicles to the bud via the actin cable network. Images were also acquired using Andor BC43 table-top spinning disk confocal system using a 60x oil objective and scMOS camera detection. Images were deconvolved using Andor Fusion software and any adjustments for representation were done using Fiji (ImageJ)[78].

Mitochondrial morphology

Mitochondrial morphology was assessed with Om45-3xmCherry tagged at its genomic locus or Su9-mNeonGreen expressed from an integrated plasmid as a mitochondrial marker during imaging. Z-stacks of mid-log phase cells were acquired using Olympus IX83 widefield fluorescence microscope system and images were processed using the Mitochondria Analyzer plug-in in Fiji[78] to quantify mitochondrial morphology.

Retrograde Actin Cable Flow

Retrograde actin cable flow was assessed using a genomic C-terminal fusion of yeGFP to Abp140. Time-lapse images of Abp140-yeGFP expressing cells were acquired at an interval of 1 sec for 15 cycles with a 63x oil objective using Andor Dragonfly 502 spinning disk confocal system. Images were analyzed to measure rate of actin cable elongation towards the rear of the mother cell.

Latrunculin B sensitivity assay

Yeast cells were grown to mid-log phase at 25°C and LatB (SigmaAldrich, cat. No.: 428020) was added to a final concentration of 67μM. Cells were fixed with 4% paraformaldehyde at time points 0 min, 2 min and 04.30 min after LatB addition. The cells were then stained with Alexa488-phalloidin and imaged as described above.

Image analysis and statistical analysis

All images were processed using Fiji (ImageJ)[78]. The specific analysis pipelines are mentioned in the above sections for each type of measurement. The graphs were plotted using GraphPad Prism (v.6.04) and statistical tests were also performed using in-built functions in GraphPad Prism. * $p < 0.05$, ** $p < 0.01$, *** $p < 0.001$, ****$p < 0.0001$

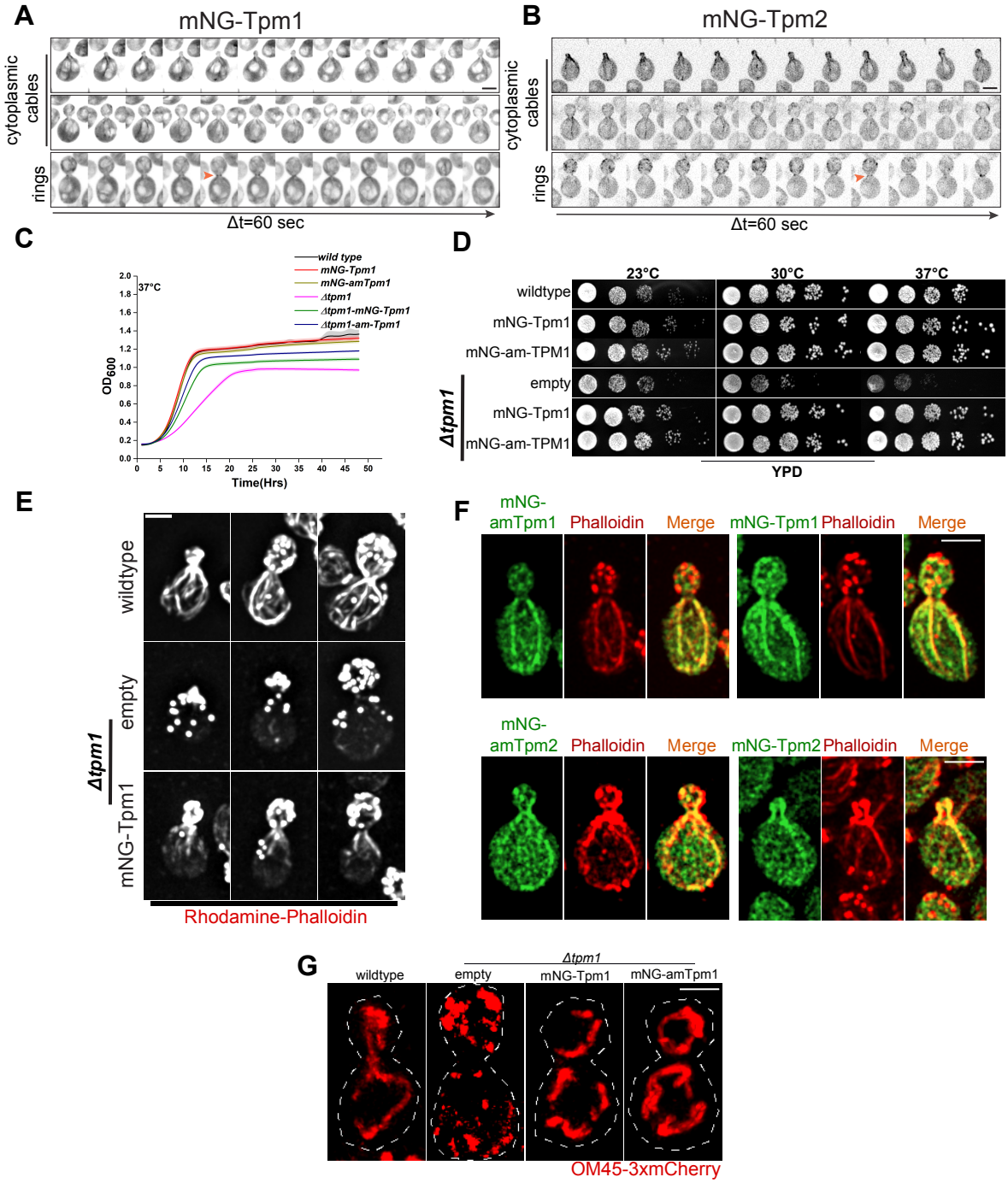

Figure S1: Functional characterization of mNeonGreen-Tpm fusion proteins. (A) Representative time-lapse montages of wildtype yeast cells expressing mNG-Tpm1; scale bar - 3μm. **(B)** Representative time-lapse montages of wildtype yeast cells expressing mNG-Tpm2; scale bar - 3μm. **(C)** Plot representing growth curves of indicated yeast strains performed at 37°C. y-axis represents mean absorbance at 600nm. **(D)** Spot assay image for indicated yeast strains performed at 23°C, 30°C, and 37°C. **(E)** Representative images of cells of indicated yeast strains stained with Rhodamine-phalloidin; scale bar – 2μm. **(F)** Representative images of cells expressing indicated mNeonGreen-Tpm fusion proteins stained with Rhodamine-phalloidin; scale bar - 2μm. **(G)** Representative images of indicated yeast strains expressing Om45-3xmCherry from the native locus; scale bar - 2μm.

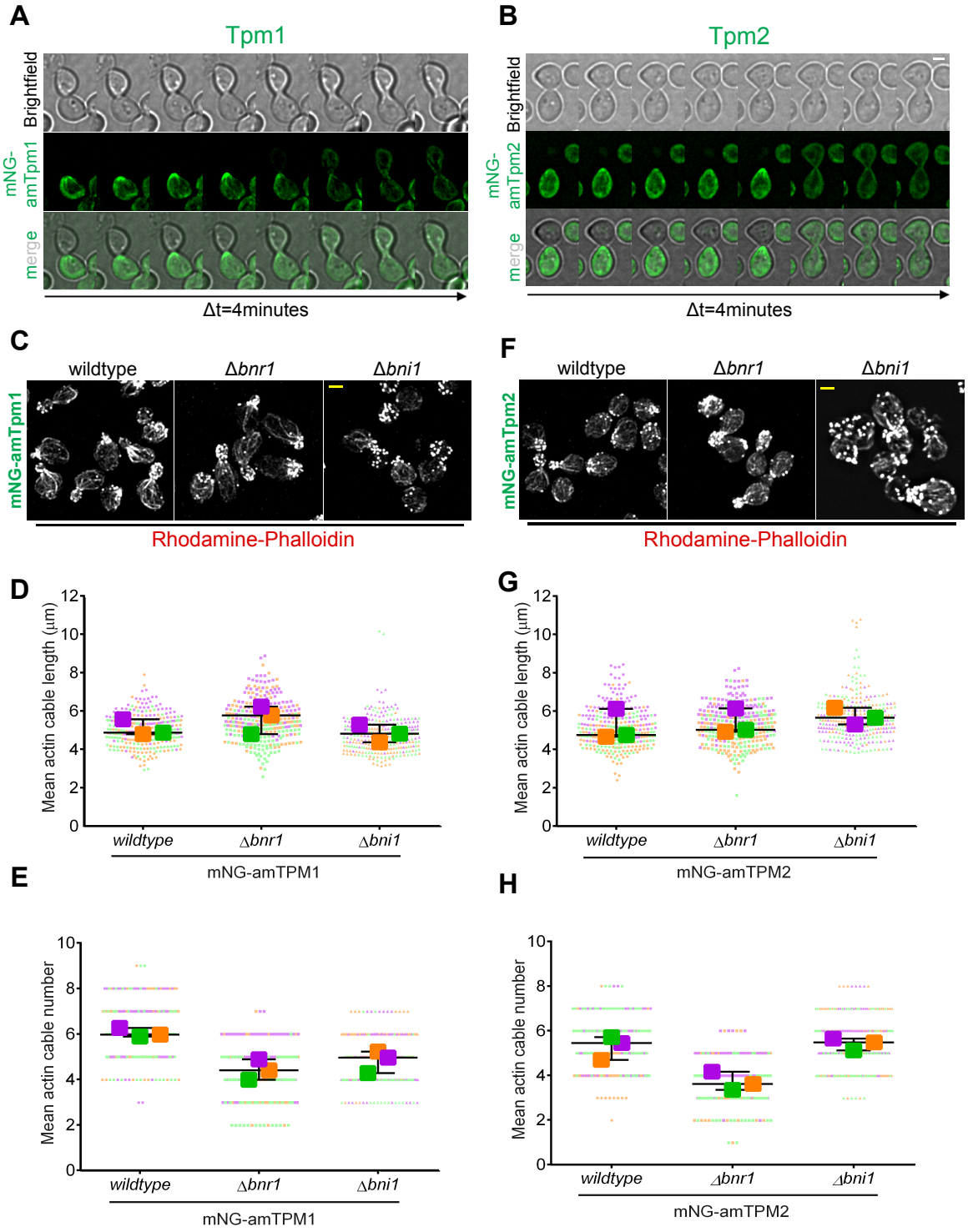

Figure S2: Tpm1 and Tpm2 co-localize at the fusion focus in mating yeast cells. (A) Representative time-lapse montages of haploid *MATa* type wildtype yeast cell expressing mNG-amTpm1 mating with haploid *MATα* wildtype yeast cell; scale bar – 2µm. **(B)** Representative time-lapse montages of haploid *MATa* type wildtype yeast cell expressing mNG-amTpm2 mating with haploid *MATα* wildtype yeast cell; scale bar – 2µm. **(C)** Representative images of cells of wildtype, Δ*bnr1*, and Δ*bni1* cells expressing mNG-amTpm1 stained with Rhodamine-phalloidin; scale bar - 2µm. **(D)** Superplot representing mean actin cable length per cell in wildtype, Δ*bnr1*, and Δ*bni1* cells expressing mNG-amTpm1; n=100 cells per strain per replicate, N=3. **(E)** Superplot representing mean actin cable number per cell in wildtype, Δ*bnr1*, and Δ*bni1* cells expressing mNG-amTpm1; n=100 per strain per replicate, N=3. **(F)** Representative images of cells of wildtype, Δ*bnr1*, and Δ*bni1* cells expressing mNG-amTpm2 stained with Rhodamine-phalloidin; scale bar – 2µm. **(G)** Superplot representing mean actin cable length per cell in wildtype, Δ*bnr1*, and Δ*bni1* cells expressing mNG-amTpm2; n=100 cells per strain per replicate, N=3. **(H)** Superplot representing mean actin cable number per cell in wildtype, Δ*bnr1*, and Δ*bni1* cells expressing mNG-amTpm2; n=100 cells per strain per replicate, N=3.

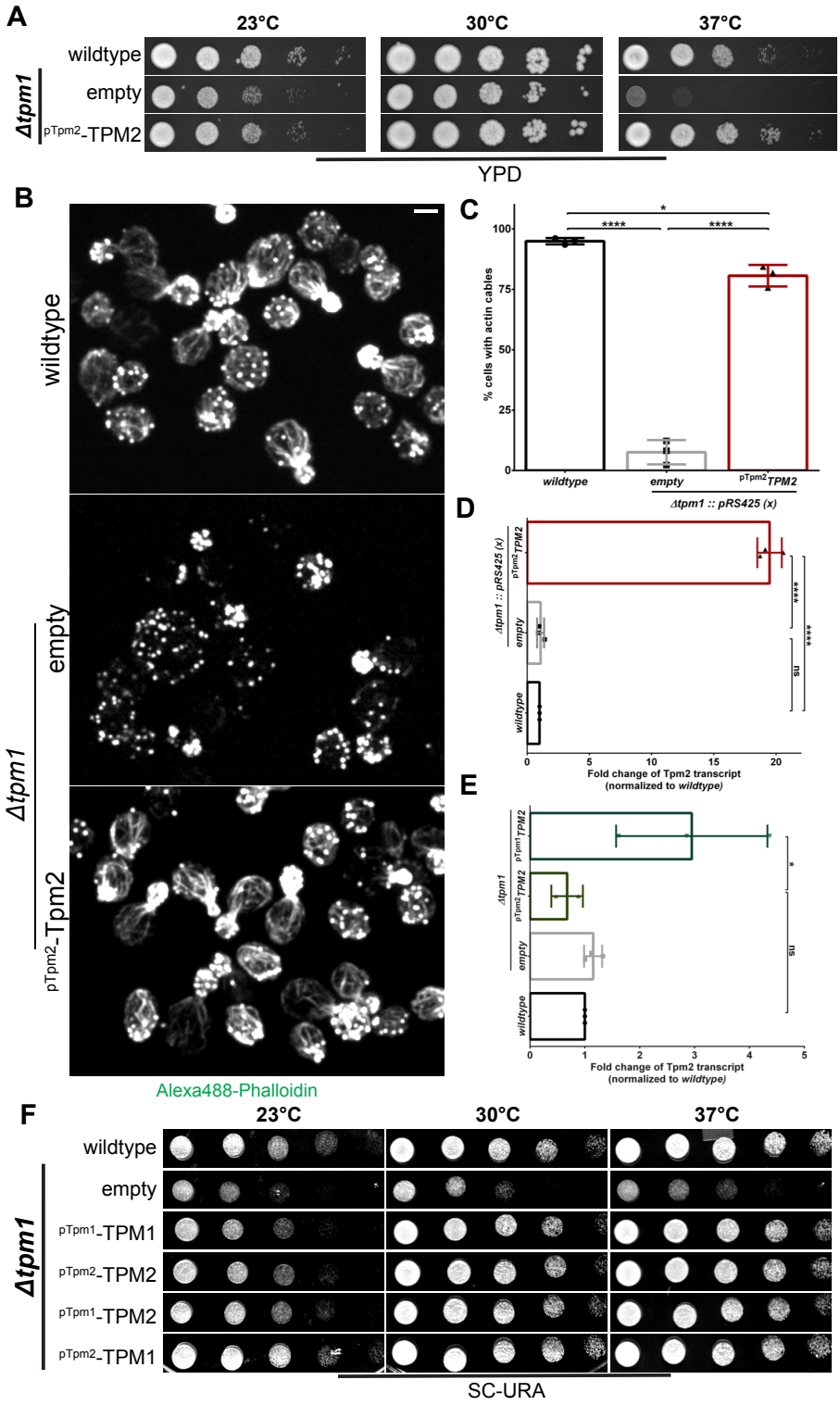

Figure S3: Tpm2 overexpression restores actin cables in *Δtpm1* cells. (A) Spot assay image for indicated yeast strains performed at 23°C, 30°C, and 37°C. **(B)** Representative images of indicated yeast strains stained with Alexa488-phalloidin; scale bar – 2μm. **(C)** Plot representing mean percentage of cells with detectable actin cables in indicated yeast strains averaged over 3 biological replicates; n≥200 cells for each strain per replicate, N=3. **(D)** Plot representing fold change of Tpm2 transcript levels normalized to wildtype in the indicated yeast strains; n=3 per strain per experiment, N=3. **(E)** Plot representing fold change of Tpm2 transcript levels normalized to *wildtype* in the indicated yeast strains; n=3 per strain per experiment, N=3. **(F)** Spot assay image for indicated yeast strains performed at 23°C, 30°C, and 37°C.
*Box represents 25th and 75th percentile, line represents median, whiskers represent minimum and maximum value.

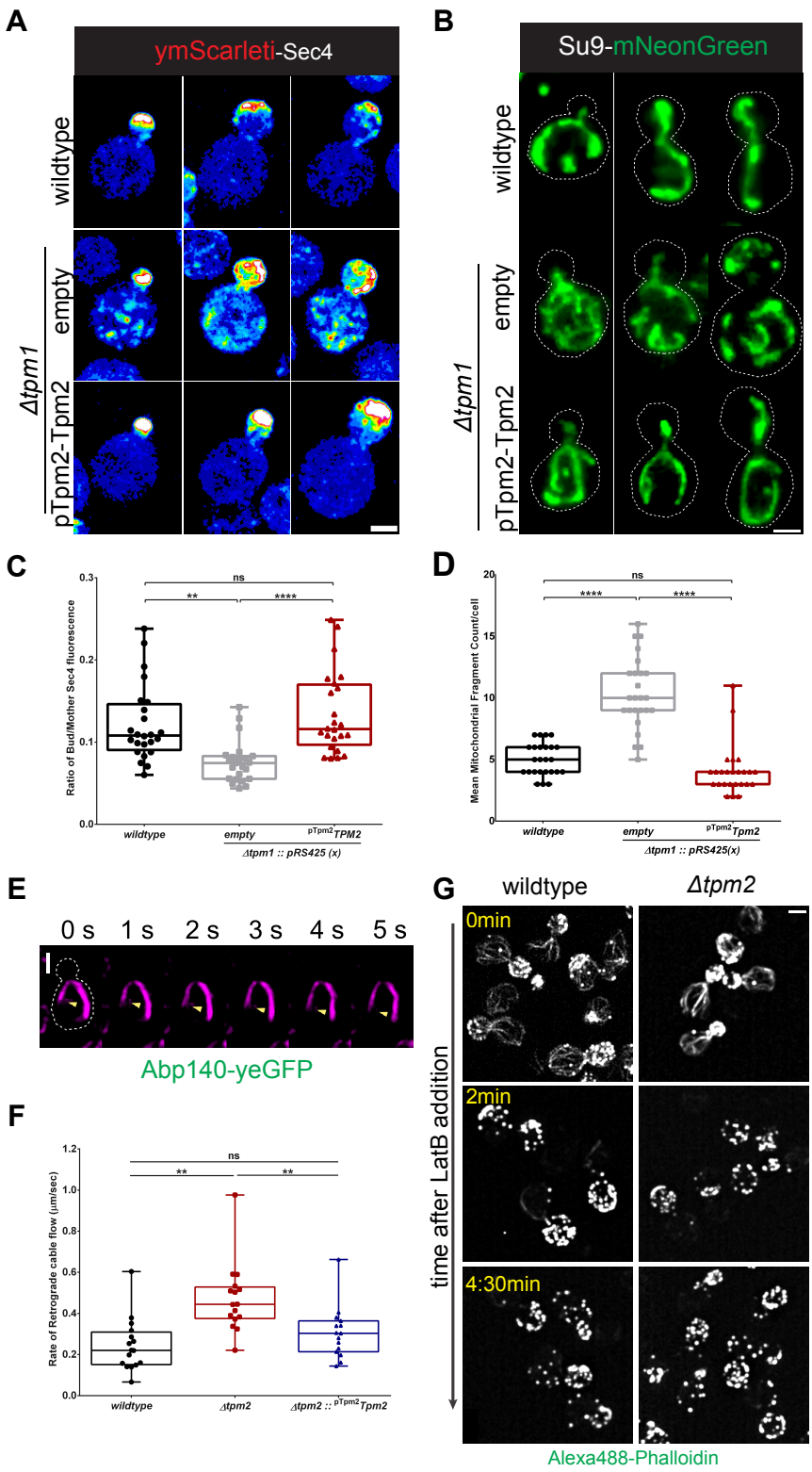

Figure S4: Tpm2 overexpression restores actin cable dependent functions in *Δtpm1* cells. (A) Representative images of indicated yeast strains expressing ymScarleti-Sec4; scale bar – 2µm. **(B)** Representative images of indicated yeast strains expressing Su9-mNeonGreen; scale bar – 2µm. **(C)** Plot representing ratio of bud/mother ymScarleti-Sec4 fluorescence per cell in the indicated yeast strains; n≥24 cells per strain. **(D)** Plot representing mean mitochondrial fragment count per cell in the indicated yeast strains; n≥25 cells per strain. **(E)** Representative time-lapse montages of wildtype yeast cells expressing Abp140-yeGFP from its native locus, scale bar - 2µm. **(F)** Plot representing retrograde actin cable flow rate (µm/s) in the indicated yeast strains; n≥15 cells per strain. **(G)** Representative time-course images of wildtype and Δ*tpm2* cells treated with Latrunculin B (67µM) and stained with Alexa488-phalloidin; scale bar - 2µm.
*Box represents 25th and 75th percentile, line represents median, whiskers represent minimum and maximum value